Acoustically Driving the Single Quantum Spin Transition of Diamond Nitrogen-Vacancy Centers

CNF Project Number: 2126-12

Principal Investigator(s): Gregory D. Fuchs[1]

User(s): Huiyao Chen[2], Johnathan Kuan[2]

Affiliation(s): 1. School of Applied and Engineering Physics, 2. Department of Physics; Cornell University

Primary Source(s) of Research Funding: DARPA DRINQS program (Cooperative Agreement #D18AC00024); Office of Naval Research (Grants No. N000141712290)

Contact: gdf9@cornell.edu, hc846@cornell.edu, jk2788@cornell.edu

Website: http://fuchs.research.engineering.cornell.edu

Primary CNF Tools Used: PT770 etcher, GCA 5x stepper, Heidelberg mask writer DWL2000, AJA sputtering deposition System, odd/even evaporator, YES asher, P10 profilometer, Westbond 7400A ultrasonic wire bonder

Abstract:

Using a high quality factor 3 GHz bulk acoustic wave resonator device, we demonstrate the acoustically driven single quantum (SQ) spin transition ($|m_s = 0\rangle \leftrightarrow |\pm 1\rangle$) for diamond nitrogen-vacancy (NV) centers and characterize the corresponding stress susceptibility. We find that the SQ spin-stress coupling is comparable to that for double quantum (DQ) transition, about an order of magnitude larger than a theoretical prediction. This work further completes our understanding of the NV spin-stress Hamiltonian and enables all-acoustic spin control of NV center spins.

Summary of Research:

Acoustic control of diamond nitrogen-vacancy (NV) center spins provides additional resources for quantum control and coherence protection that are unavailable in conventional magnetic resonance approaches. While acoustically-driven double quantum spin transition has been widely studied, acoustically-driven single quantum spin transition is yet unexplored.

Here we report our experimental study of acoustically-driven SQ spin transitions of NV centers using a 3 GHz diamond bulk acoustic resonator device [1]. The device converts a microwave driving voltage into an acoustic wave through a piezoelectric transducer, thus mechanically addressing the NV centers in the bulk diamond substrate (Figure 1). Because a microwave current flows through the device transducer, an oscillating magnetic field of the same frequency coexists with the stress field that couples to SQ spin transitions.

To identify and quantify the mechanical contribution to the SQ spin transition, we use Rabi spectroscopy to separately quantify the magnetic and stress fields present in our device as a function of driving frequency. The results are shown in Figure 2. Based on these results, we construct a theoretical model and simulate the SQ spin transition Rabi spectroscopy to compare to the experimental results. From a systematically identified closest match (Figure 3), we quantify the mechanical driving field contribution and extract the effective spin-stress susceptibility, b'. We perform measurements on both the $|0\rangle \leftrightarrow |+1\rangle$ and $|0\rangle \leftrightarrow |-1$. SQ spin transitions and obtain $b'/b = \sqrt{2}(0.5 \pm 0.2)$, where b is the spin-stress susceptibility of DQ transition.

The fact that b' is comparable to b, about an order of magnitude larger than expected theoretically [2], has important implications for applications. It raises the possibility of all-acoustic spin control of NV centers within their full spin manifold without the need for a magnetic antenna. For sensing applications, a diamond bulk acoustic device can be practical and outperform a microwave antenna in several aspects: 1) Acoustics waves provide direct access to all three qubit transitions, and the DQ qubit enables better sensitivity in magnetic metrology applications; 2) The micron-scale phonon wavelength is ideal for local selective spin control of NV centers; 3) Bulk acoustic waves contain a uniform stress mode profile and thus allows uniform field control of a large planar spin ensemble, for example, from a delta-doped diamond growth process.

This study [3], combined with previously demonstrated phonon-driven DQ quantum control and improvements in diamond mechanical resonator engineering, shows that diamond acoustic devices are a powerful tool for full quantum state control of NV center spins.

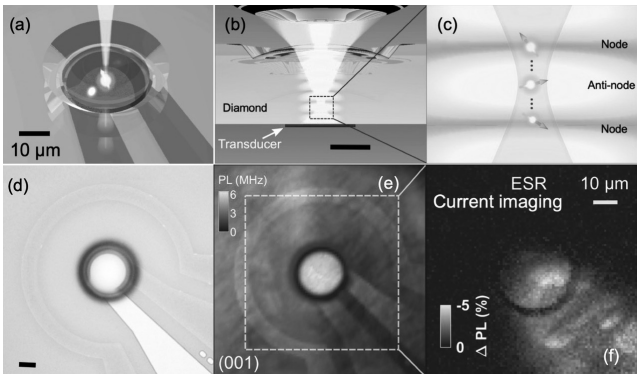

Figure 1: (a) and (b) are concept images of the device side view and cross-sectional view. An NA = 0.8 objective focuses the 532 nm laser down into diamond at a depth close to the transducer (around 3 μm in distance). The orange standing wave field illustrates the acoustic wave mode. (c) Closeup of the area under study. (d) and (e) are optical image and photoluminescence scan of the device, consisting of a semi-confocal diamond bulk acoustic resonator (center bright region) and a 50 μm radius microwave loop antenna. (f) Electron spin resonance signal mapping of the device current field around the resonator, showing current flow primarily along the electrodes.

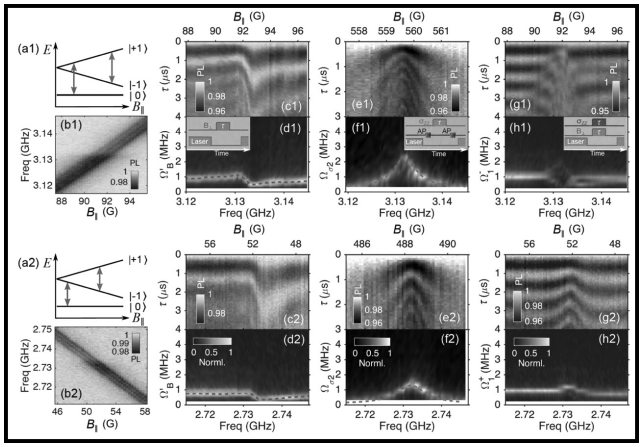

Figure 2: Spectroscopy study of NV center spin under driving fields at frequencies near two acoustic modes at (1) 3.132 GHz and (2) 2.732 GHz. Ground-state spin level diagrams in (a1-a2) show the targeted DQ (orange arrow, $|-1\rangle \leftrightarrow |+1\rangle$) and SQ (blue arrow $|0\rangle \leftrightarrow |\pm1\rangle$) transitions within nuclear spin $|m_I = +1\rangle$ hyperfine manifold. Transducer driving creates both magnetic, $B_\perp$, and acoustic fields, σ_{zz}, in the device, which can be measured independently by (c) SQ Rabi spectroscopy near the leads and (e) DQ Rabi spectroscopy in the center of the resonator. In the resonator, the two vector fields add coherently and drive the SQ transition together. Measurements of the resulting total field probed by SQ ESR and Rabi spectroscopy are shown in (b) and (g), respectively. (d, f, h) are Fourier transforms of (c, e, g). The insets in (d1, f1, h1) show the corresponding measurement sequences.

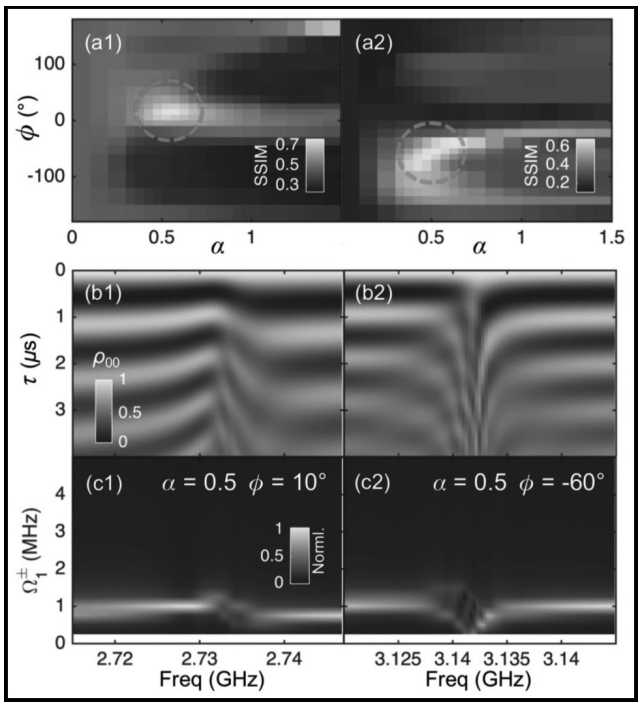

Figure 3: Quantum master simulation of SQ spin transition under dual field driving. (a1-a2) are heatmaps of structural similarity index measure between experimental data and simulation in {φ,α} parameter space for 2.732 GHz and 3.132 GHz mode, respectively. The dashed circles mark the locations of peak SSIM values. (b1-b2) The corresponding simulated Rabi spectroscopy results using the peak SSIM associated {φ,α} values match the experimental data in Figure 2g. (c1-c2) are Fourier transforms of (b1-b2).

References:

[1] H. Chen, N. F. Opondo, B. Jiang, E. R. MacQuarrie, R. S. Daveau, S. A. Bhave, and G. D. Fuchs, Nano letters 19, 7021 (2019).

[2] P. Udvarhelyi, V. O. Shkolnikov, A. Gali, G. Burkard, and A. Palyi, Physical Review B 98, 075201 (2018).

[3] H. Chen, S. Bhave, and G. Fuchs, arXiv preprint arXiv:2003.03418 (2020).

(See pages vi-vii for full color versions of all three figures.)